IEEE Photonics Journal
An IEEE Photonics Society Publication

Open Access

Performance Investigation of Underwater Wireless Optical Communication System Using *M*-ary OAMSK Modulation Over Oceanic Turbulence

Volume 9, Number 5, October 2017

Wei Wang
Ping Wang
Tian Cao
Hongxin Tian
Yan Zhang
Lixin Guo, ***Member, IEEE***

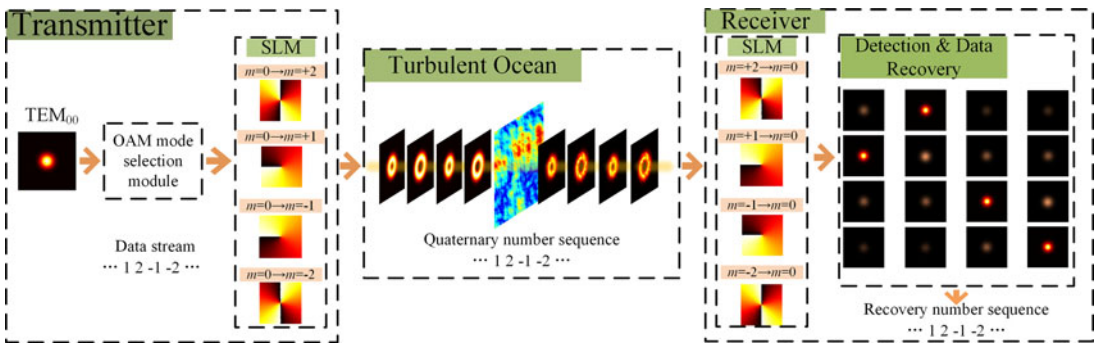

DOI: 10.1109/JPHOT.2017.2727505
1943-0655 © 2017 IEEE

IEEE photonics SOCIETY

IEEE

Performance Investigation of Underwater Wireless Optical Communication System Using *M*-ary OAMSK Modulation Over Oceanic Turbulence

Wei Wang,[1] Ping Wang,[1,2] Tian Cao,[1] Hongxin Tian,[1] Yan Zhang,[1] and Lixin Guo,[1,2] *Member, IEEE*

[1]State Key Laboratory of Integrated Service Networks, School of Telecommunications Engineering, Xidian University, Xi'an 710071, China
[2]School of Physics and Optoelectronic Engineering, Xidian University, Xi'an 710071, China

DOI:10.1109/JPHOT.2017.2727505

Manuscript received June 9, 2017; revised July 10, 2017; accepted July 12, 2017. Date of publication July 17, 2017; date of current version July 28, 2017. This work was supported in part by the National Natural Science Foundation of China under Grant 61474090, in part by the Fundamental Research Funds for the Central Universities under Grant JB160105, and in part by the 111 Project of China under Grant B08038. Corresponding author: Ping Wang (e-mail: pingwang@xidian.edu.cn).

Abstract: The performance of *M*-ary orbital angular momentum-shift keying (OAMSK) modulation-based underwater wireless optical communication (UWOC) system is investigated over oceanic turbulence with Laguerre–Gauss beam considered. On the basis of Rytov approximation, the detection probability and power distribution among the received signals are derived. The conditional probability and symbol error rate (SER) are, then, achieved by the maximum likelihood estimation. With Blahut–Arimoto algorithm, the channel capacity for this UWOC system is obtained. The results show that the optimal transmitted OAM mode set S is mainly restricted by the interfering energy and decaying effective energy. With the optimal mode interval achieved, the SER performances for different modulation orders M and the minimum required transmitting power to reach the SER of $P_e = 10^{-9}$ are sensitive to the variation in oceanic turbulence conditions. Additionally, the value of capacity will shift to a higher value with the increasing M, and a suitable M should be selected to balance the transmitting power consumption and capacity gain. This work is beneficial to *M*-ary OAMSK modulation-based UWOC system design.

Index Terms: Oceanic turbulence, underwater wireless optical communication, modulation, orbital angular momentum.

1. Introduction

In recent years, underwater explorations are gaining increasing attention to meet the demands for scientific, environmental, commercial, and military purposes, which usually require high-speed and real-time data transmission. Traditionally, those requirements can be satisfied by optical fiber and copper cable. However, wire communication is inconvenient, high costs of maintenance, and incompatible with many smaller, new devices [1]. These disadvantages necessitate design of appropriate and efficient underwater wireless communication systems, which are relatively maintenance-free and uncomplicated to set up [2]. Acoustic communication, one of the important underwater wireless communication technologies, has low attenuation in water and is capable of long-range

communication. As relatively mature and robust technologies, acoustic techniques have been well established and developed in these years [3], [4]. However, it suffers from limited data rates and high latency due to the speed of sound in water [1]. In contrast, the underwater wireless optical communication (UWOC), possesses higher data rates (10 Mbps or more), lower time latency, and better security [2], [5]. And it has been proposed as a good alternative or complementary solution to the existing acoustic communication technology for underwater applications [1], [6]–[9]. Recently, some progress has been made on UWOC system modeling, design and development with different modulation schemes [10]–[16]. Jaruwatanadilok *et al.* in [14] presented a theoretical investigation of an UWOC system with on-off keying (OOK) modulation. The study showed that OOK modulation outperforms 4-level amplitude modulation (AM) in bit-error-rate (BER) performance. Cox *et al.* in [15] demonstrated a low-cost and simple design for transmitting and receiving polarized optical signals in underwater channel. This system was successfully tested using a binary polarization-shift keying (BPolSK) modulation scheme to send data over an underwater optical link. Sui *et al.* in [16] evaluated the phase shift keying PSK modulation technique for UWOC system. The simulated results of BER, power efficiency, data rates and implementation complexity are discussed and compared. It is shown that the phase shift keying (PSK) is suitable candidates for underwater wireless optical link applications. Oubei *et al.* in [17] showed an UWOC system employing orthogonal frequency division multiplexed quadrature amplitude modulation (QAM-OFDM), which achieved a record data rate of up to 4.8 Gbit/s over 5.4-m transmission distance. As is known, for these modulation schemes adopted, several photon degrees of freedom [17] have been employed, such as amplitude in OOK-NRZ [12], polarization in BPolSK modulation [15], phase in PSK modulation [16], and subcarrier in QAM-OFDM [12]. Apart from those photon degrees of freedom, Gibson *et al.* in [18] proposed another encoding (modulation) scheme employing a new photon degree of freedom, which is orbital angular momentum (OAM) and structurally independent of the photon degrees of freedom applied to those modulation methods above. Actually, OAM is associated with the helicity of phasefronts of light beams. Each photo with OAM mode contains the helical phase front $\exp(im\varphi)$ ($m = 0, \pm 1, \pm 2, \ldots$) and can carry an OAM of $m\hbar$ per photon, where $\hbar$ is the reduced Planck constant [17]–[21]. OAM modes with different values of m are orthogonal to each other, which will allow them to provide an orthogonal modal basis set [19]. Besides, sampling the beam away from its axis may suffer from angular restriction because it requires a measurement aperture without any angular restriction to receive OAM signals, which shows that the OAM-based modulation communication system possesses more tolerance to eavesdropping [22]. These advantages make OAM-based modulation scheme quite attractive in optical wireless communication systems. Very recently, some works of OAM-based modulation (encoding) have been reported over atmospheric turbulent and non-turbulent channels. Krenn *et al.* in [23] experimentally analyzed the transmission of OAM modes through 3 km of strong turbulence over Vienna employing an incoherent detection scheme with adaptive optical systems. It indicated that different OAM mode superpositions could be distinguished with a very low average error rate. Du *et al.* in [24] experimentally demonstrated an *M*-ary coding free-space optical communication system employing visible vortex Bessel beams over 12-m distance. It showed that the measured BER of hexadecimal coding/decoding remains zero even with an opaque obstruction placed. Willner *et al.* in [25] showed a schematic overview of an OAM-based encoding system. They indicated that for a fixed optical power, a higher amount of data can be modulated if there are more possible modes to occupy (i.e., higher modulation order to employ) in one symbol time. Kai *et al.* in [26] proposed a free space communication system based on orbital angular momentum shift keying modulation. They transmitted an image encoded by a set of OAM states at the transmitter equipped with multiplexing phase hologram. After free space transmission, the recovered image showed a high fidelity to the original image at the receiver equipped with a novel phase hologram. However, there is no literature reported on the performance investigation of turbulent UWOC system with OAM-based modulation scheme up to now, to the best of our knowledge.

In this work, the performance of an M-ary UWOC system employing vortex Laguerre-Gauss (LG) beam with orbital angular momentum-shift keying (OAMSK) modulation over weak oceanic turbulent channels is studied. The properties of LG beams with various OAM modes propagating in weak

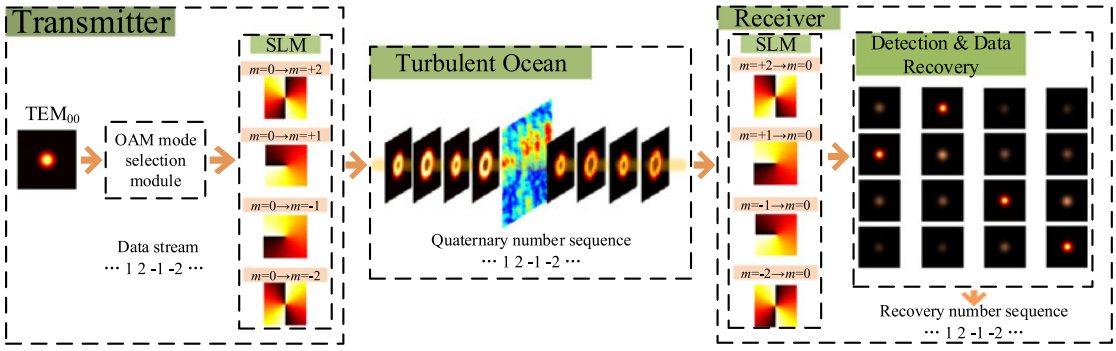

Fig. 1. Proposed quaternary OAMSK modulation-based UWOC system.

turbulent ocean are obtained on the basis of Rytov approximation theory. After that, the analytical expressions for the symbol error rate (SER) and channel capacity of OAMSK modulation-based UWOC system are derived, respectively. Then, with the optimal mode interval Δm computed, the SER performances and channel capacity of this M-ary UWOC system under different weak turbulence conditions are analyzed in detail.

2. OAMSK Modulation UWOC System and Propagation in Oceanic Turbulence

2.1 OAMSK Modulation Scheme

Fig. 1 depicts the operation principle of UWOC system using quaternary OAMSK modulation/demodulation. Each quaternary symbol is corresponding to an OAM mode with a topological number m (e.g., $00 \rightarrow m_1$, $01 \rightarrow m_2$, $10 \rightarrow m_3$, and $11 \rightarrow m_4$) uniquely. At the transmitter, in a symbol period T, a light beam with OAM mode number $m = 0$ is selectively launched onto a programmable spatial light modulator (SLM) by the OAM mode selection module. This SLM is loaded with a specific spiral phase hologram corresponding to the quaternary symbol which will be transmitted in T [27]. Then, the incoming beam is converted into the desired vortex beam with a specific topological number in the mode set (e.g., $m_1 = -2$, $m_2 = -1$, $m_3 = 1$, $m_4 = 2$). Modulated by SLM, the time-varying light beam carrying 2 bits of information is sent to the receiver through turbulent UWOC channel and will be interfered by oceanic turbulence. At the receiver, an OAM mode m_i ($i = 1, 2, 3, 4$) would be demodulated and converted into $m = 0$ by introducing the inverted spiral phase hologram $-m$ into SLM. When an OAM beam is detected, it will be demodulated with all the possible inverted spiral phases in the mode set ($-m_1 = 2, -m_2 = 1$, $-m_3 = -1$, $-m_4 = -2$), respectively [24]. Here, take the demodulation process of mode m_1 as an example. If the OAM beam with mode m_1 can be demodulated with its corresponding inverted spiral phase $-m_1$, it will be converted into the original light beam with OAM mode $m = 0$ and a bright spot will appear at the center of the beam. Otherwise, the beam will be converted into the one with OAM mode $m_1 - m_i$ ($i = 1, 2, 3$) and the center of the beam remains dark. In addition, the oceanic turbulence-induced extrinsic beam can also be detected, thus leading to an interfering dim spot at the center of interfering beam. After being demodulated, the effective and interfering beams with OAM mode of 0 will be changed into electrical current and sampled. Then, the symbol with the largest sampling value can be determined as original transmitting symbol by the decision device. Thus, the original quaternary sequence can be recovered one by one.

2.2 Properties of Laguerre–Gauss Beams in Oceanic Turbulence

Laguerre-Gauss (LG) beams are widely used among the optical beams carrying OAM because they are easy to be used and implemented [28]. In ocean without turbulence, the optical field distribution

of LG beams at the waist plane with propagation distance z can be written as

$$L\,G_m^{free}(\rho,\varphi,z) = R_m(\rho,z)\exp(-im\varphi), \tag{1}$$

where (ρ,φ,z) denotes cylindrical coordinates, m is the angular index of the OAM mode, and $R_m(\rho,z)$ represents radial function, which can be expressed as

$$R_m(\rho,z) = \sqrt{\frac{2p!}{\pi(p+|m|)!}}\frac{1}{\omega(z)}\left[\frac{\rho\sqrt{2}}{\omega(z)}\right]^{|m|}\exp\left[\frac{-\rho^2}{\omega^2(z)}\right]L_p^m\left[\frac{2\rho^2}{\omega^2(z)}\right] \times \exp\left[\frac{-ik\rho^2 z}{2\left(z^2+z_R^2\right)}\right]\exp\left[i(2p+|m|+1)\tan^{-1}\frac{z}{z_R}\right], \tag{2}$$

where $\omega(z)=\omega_0\sqrt{1+(z/z_R)^2}$ represents the beam radius at distance z, in which ω_0 is the radius of the zero-order Gaussian beam at the waist, $z_R=\pi\omega_0^2/\lambda$ is the Rayleigh range, λ is the optical wavelength, and $k=2\pi/\lambda$ is the propagation constant [28]. $L_p^m(\cdot)$ stands for the generalized Laguerre polynomial, and when p equals zero, $L_p^m(\cdot)$ will be unity. Here, it should be noted that (1) will be reduced to the TEM_{00} mode with $m=0$ [29]. In this work, without loss of generality, p is assumed to be zero.

When turbulence is taken into account, inhomogeneities in temperature and salinity of ocean will lead to random change of refractive index, which may alter the angular momentum of beams and the helical wave front phase profile of beams will be distorted. In the weak oceanic turbulence region, on the basis of the Rytov approximation, the optical field of a propagated Laguerre-Gauss beam can be written with the help of [30] as

$$L\,G_m^T(\rho,\varphi,z) \approx L\,G_m^{free}(\rho,\varphi,z)\exp[\psi_m(\rho,\varphi,z)], \tag{3}$$

where $\psi_m(\rho,\varphi,z)$ is the oceanic turbulence-induced complex phase perturbation.

After propagating through a weak oceanic turbulent channel, the transmitted LG beam with OAM mode m will diverge to several LG beams with different OAM modes. Thus, $L\,G_m^T(\rho,\varphi,z)$ can be expressed as a Fourier series

$$\begin{aligned} L\,G_m^T(\rho,\varphi,z) &= \sum_{n=-\infty}^{+\infty} L\,G_{m\to n}(\rho,\varphi,z) \\ &= \sum_{n=-\infty}^{+\infty} \alpha_n(\rho,z)\,L\,G_n^{free}(\rho,\varphi,z) \\ &= \sum_{n=-\infty}^{+\infty} [\alpha_n(\rho,z)\,R_n(\rho,z)]\exp(-in\varphi). \end{aligned} \tag{4}$$

Eq. (4) shows that the receiver will detect a linear superposition of various beams with different OAM modes, where $L\,G_{m\to n}(\rho,\varphi,z)$ is the part of original beam diverging to beam with OAM mode n and $\alpha_n(\rho,z)$ is the superposition coefficient of LG beams with OAM mode n. Then, $\alpha_n(\rho,z)$ can be further given as

$$\begin{aligned} \alpha_n(\rho,z) &= \frac{IDTFT\left[L\,G_m^T(\rho,\varphi,z)\right]}{R_n(\rho,z)} \\ &= \frac{1}{2\pi R_n(\rho,z)}\int_0^{2\pi} L\,G_m^T(\rho,\varphi,z)\exp(in\varphi)\,d\varphi. \end{aligned} \tag{5}$$

Eq. (5) shows that the stochastic nature of oceanic turbulence will lead to the random quantity of $\alpha_n(\rho,z)$. If the intensity of LG beam described by $I_n=\iint L\,G_n^*(\rho,\varphi,z)L\,G_n(\rho,\varphi,z)\rho d\rho d\varphi$ is adopted, the normalized shifted energy $\eta_{n,m}$, which is the energy shifted from the original OAM mode m into

extrinsic mode n, and the effective energy $\eta_{m,m}$, which represents the energy remaining in original mode m, can be calculated via (6) and written as

$$\eta_{n,m} = \frac{\langle I_{n,m}\rangle_T}{\sum_{k=-\infty}^{+\infty}\langle I_{k,m}\rangle_T} \tag{6}$$

with

$$\langle I_{n,m}\rangle_T = \left\langle \iint L\,G^*_{m\to n}(\rho,\varphi,z)\,L\,G_{m\to n}(\rho,\varphi,z)\,\rho \mathrm{d}\rho\mathrm{d}\varphi \right\rangle_T, \tag{7}$$

where the operator $\langle\cdot\rangle_T$ represents the ensemble average over the oceanic turbulence channel, $\langle I_{n,m}\rangle_T$ is the normalized average shifted energy with transmitting power $I_m = 1$. Considering the nature of orthogonality among LG beams with different OAM modes, the scalar product of two optical fields with different OAM modes can be calculated and expressed as

$$\iint L\,G^{free}_m(\rho,\varphi,z)\,L\,G^{free,*}_n(\rho,\varphi,z)\rho \mathrm{d}\rho\mathrm{d}\phi = \begin{cases} 0 & \forall n \neq m \\ I_m & n = m \end{cases}, \tag{8}$$

and

$$\begin{aligned} &\iint L\,G^*_{m\to n}(\rho,\varphi,z)\,L\,G_{m\to n}(\rho,\varphi,z)\,\rho \mathrm{d}\rho\mathrm{d}\varphi \\ &= \iint \left[\sum_{n=-\infty}^{+\infty} L\,G^*_{m\to n}(\rho,\varphi,z)\right] L\,G_{m\to n}(\rho,\varphi,z)\,\rho \mathrm{d}\rho\mathrm{d}\varphi \\ &= \iint L\,G^{T,*}_m(\rho,\varphi,z)\,L\,G_{m\to n}(\rho,\varphi,z)\,\rho \mathrm{d}\rho\mathrm{d}\varphi. \end{aligned} \tag{9}$$

Substituting $L\,G_{m\to n}(\rho,\varphi,z)$ in (9) with (4), the normalized average shifted energy can be rewritten as

$$\langle I_{n,m}\rangle_T = \left\langle \iint L\,G^{T,*}_m(\rho,\varphi,z)\left[\alpha_n(\rho,z)\,R_n(\rho,z)\right]\exp(-in\varphi)\,\rho \mathrm{d}\rho\mathrm{d}\varphi \right\rangle_T. \tag{10}$$

Then, substituting (5) into (10), $\langle I_{n,m}\rangle_T$ can be further achieved with the help of [31], [32] as

$$\begin{aligned} \langle I_{n,m}\rangle_T &= \left\langle \iint L\,G^{T,*}_m(\rho,\varphi,z)\exp(-in\varphi) \right. \\ &\quad \left. \times \left[\frac{1}{2\pi}\int L\,G^T_m(\rho,\varphi',z)\exp(in\varphi')\,d\varphi'\right]\rho \mathrm{d}\rho\mathrm{d}\varphi \right\rangle_T \\ &= \frac{1}{2\pi}\iiint L\,G^{free,*}_m(\rho,\varphi,z)\,L\,G^{free}_m(\rho,\varphi',z)\exp\left[in(\varphi'-\varphi)\right] \\ &\quad \times \left\langle \exp[\psi^*(\rho,\varphi,z)+\psi(\rho,\varphi',z)]\right\rangle_T \rho \mathrm{d}\rho\mathrm{d}\varphi\mathrm{d}\varphi' \\ &= \frac{1}{2\pi}\iiint |R_m(\rho,z)|^2\exp\left[i(n-m)\Delta\varphi\right] \\ &\quad \times \exp\left[2\rho^2(\cos\Delta\varphi-1)\times k^2 z\mathrm{T}(\varsigma,\varepsilon,\chi_T,\tau)\right]\rho \mathrm{d}\rho\mathrm{d}\Delta\varphi, \end{aligned} \tag{11}$$

where $\mathrm{T}(\varsigma,\varepsilon,\chi_T,\tau)$ denotes the strength of the oceanic turbulence and can be expressed with the help of [33] as

$$\mathrm{T}(\varsigma,\varepsilon,\chi_T,\tau) = \frac{\pi^2}{3}\int_0^\infty \kappa^3\Phi_{ocean}(\kappa)\,\mathrm{d}\kappa. \tag{12}$$

Here, $\Phi_{ocean}(\kappa)$ is the spatial power spectrum of the refractive index fluctuations of the oceanic water, which has been got in [34]–[36] as

$$\Phi_{ocean}(\kappa) = 0.388 \times 10^{-8}\varepsilon^{-1/3}\chi_T\kappa^{-11/3}\left[1 + 2.35(\kappa\varsigma)^{2/3}\right]\left(e^{-A_T\delta} - 2\tau^{-1}e^{-A_{Ts}\delta} + \tau^{-2}e^{-A_S\delta}\right), \quad (13)$$

where ς is the Kolmogorov inner scale, τ is the relative strength of temperature and salinity fluctuations, varying in the interval of $[-5,\ 0]$ in the oceanic water, ε is the rate of dissipation of kinetic energy per unit mass of fluid which varies in the range from $10^{-1}\mathrm{m^2s^{-3}}$ to $10^{-10}\mathrm{m^2s^{-3}}$, χ_T is the dissipation rate of temperature, which is in the range from $7 \times 10^{-10}\mathrm{K^2s^{-1}}$ to $10^{-4}\mathrm{K^2s^{-1}}$ in clean sea-water. $A_T = 1.863 \times 10^{-2}$, $A_S = 1.9 \times 10^{-4}$, $A_{TS} = 9.41 \times 10^{-3}$, and $\delta = 8.284(\kappa\varsigma)^{4/3} + 12.978(\kappa\varsigma)^2$. Following the work in [37], $C_n^2 = 10^{-8}\varepsilon^{-1/3}\chi_T$ is assumed, which is a constant and similar to the temperature structure parameter in atmospheric turbulence. Then, substituting (13) into (12), the spatial coherence length of the spherical wave propagating in the turbulence ocean can be expressed as

$$\mathrm{T}(\varsigma, \varepsilon, \chi_T, \tau) = 1.2765 \times \varsigma^{-1/3}C_n^2\left(6.78 + 47.57\tau^{-2} - 17.67\tau^{-1}\right). \quad (14)$$

On the basis of (3), the cumulative effect of weak turbulence over the propagating procedure can be regarded as a phase perturbation. Therefore, the turbulence induced intensity fluctuation can be neglected and all the energy collected by receiver can be expressed as

$$\sum_{k=-\infty}^{+\infty} I_{k,m} = I_m = 2\pi\int |R_m(\rho, z)|^2\rho\mathrm{d}\rho. \quad (15)$$

2.3 SER and Channel Capacity of OAMSK Modulation UWOC System

In this part, the analytical expressions for SER and channel capacity of OAMSK-based UWOC system are derived, respectively. Generally, an optical signal will be subjected to the attenuation caused by absorption and scattering, and distortion (fading) caused by oceanic turbulence when it propagates in turbulent ocean. To model the channel characteristics of the UWOC system, the channel impulse response with respect to turbulence, absorption and scattering are always considered [7]–[9]. In this work, it is assumed that the LG beam with OAM modes s_i in the range of $S = \{s_1, s_2, \ldots, s_i, \ldots s_M\}$ is transmitted, where S represents the transmitted OAM mode set consisting of all the modes that the OAMSK system will transmit, and M represents an M-ary system. The original transmitted OAM mode s_i propagates over weak turbulent ocean, and its energy will shift into the adjacent OAM modes (e.g., $s_j,\ s_j \in S$ and $i \neq j$) result from distortion caused by weak oceanic turbulence. The receiver collects the energy that remains in mode s_i and the energy that is shifted to extrinsic superfluous mode s_j. Furthermore, if the mode s_i diffuses into s_k, which is out of S, the energy of s_k cannot be collected by the receiver because that the spiral phase launched onto SLM for demodulation at the receiver are limited in the range of $\hat{S} = \{-s_1, -s_2, \ldots, -s_i, \ldots -s_M\}$.

In addition to oceanic turbulence-induced energy shifting, the optical signal will be attenuated in seawater by two processes, absorption and scattering. The absorption and scattering coefficients, $K_A(\lambda)$ and $K_S(\lambda)$, vary with the water type and source wavelength [38]. As is known, multiple scattering may cause temporal spread of optical signals, which therefore results in inter-symbol interference (ISI) and degrades system error performance [38]–[41]. Here, we mainly focus on the pure seawater and assume the symbol duration T is long enough compared to the maximum delay spread (typically, 10 times as big would be good enough), and then the UWOC channel can be regarded as an equivalent ISI-free channel [42]. The absorption and scattering-induced loss coefficient η_0 for ISI-free UWOC channel can be determined with the help of [43] as

$$\eta_0 = \frac{\int_0^T r(t) * p_T(t)\,\mathrm{d}t}{\int_0^T p_T(t)\,\mathrm{d}t} = \frac{\int_0^T r(t) * p_T(t)\,\mathrm{d}t}{P_T}, \quad (16)$$

where $r(t)$ is the channel impulse response with respect to the absorption and scattering effects, which can be simulated relying on Monte Carlo approach [44], [45]. $p_T(t)$ is the transmitted signal power, P_T is the total transmitted power for a symbol period, and $*$ denotes the convolution operation.

It should be noted that $r(t)$ can be modeled as an ideal delta Dirac function for the ISI-free UWOC channel on the basis of [43]. Thus, the absorption and scattering effects are modeled as a simple loss coefficient η_0.

After a LG beam with OAM mode s_i is demodulated by SLM, at the input of the photodetector, the received effective power of the LG beam can be written with the help of [38] and [46] as

$$P_{R,i}^{(s_i)} = \eta_{s_i,s_i}\eta_0 \frac{A}{\pi\theta^2 z^2} P_T,\ i \in [1, M], \tag{17}$$

where A is the area of the reception and θ is the beam divergence angle. $L = \eta_0 \frac{A}{\pi\theta^2 z^2}$ is assumed, which is a constant for given transmitted distance z and represents the path loss of the LG beam when it propagates over the turbulent ocean. And the received interfering power of extrinsic mode s_j is

$$P_{R,j}^{(s_i)} = \eta_{s_j,s_i} L\, P_T,\ j \neq i \text{ and } j \in [1, M]. \tag{18}$$

As is known, the photodetector will change light power into photocurrent with the help of photoelectric effect. Besides, at the photodetector, the impact of noise should be considered, which is a combination of background radiation noise, dark current noise, thermal noise and signal-dependent shot noise [14], [47]. Since these components are additive and independent of each other, they can be approximated and modeled as additive white Gaussian noise (AWGN) [39], [48]. Specially, on the basis of [48], the signal-dependent shot noise can be assumed to be negligible. Thus, the variance of it is independent of the received signal and considered constant. Then, the photocurrent is sampled and the average output of sampler can be expressed as

$$\begin{aligned} \langle y_o \rangle &= \langle i_o \rangle + n \\ &= \langle G_n \rangle \eta L\, P_T + n, \end{aligned} \tag{19}$$

where n represents the signal-independent additive white Gaussian noise with zero mean and variance $N/2$ [49]. Variable $\langle i_o \rangle$ equals $\langle G_n \rangle \eta L\, P_T$, where $\langle G_n \rangle$ is the average gain of the detector [50]. Thus, the received signal vector at the input of decision device is

$$\mathbf{r} = \left[\left\langle y_o^{(s_i)} \right\rangle_1, \left\langle y_o^{(s_i)} \right\rangle_2, \ldots, \left\langle y_o^{(s_i)} \right\rangle_i, \ldots, \left\langle y_o^{(s_i)} \right\rangle_M \right]. \tag{20}$$

The envelope of $\langle y_o^{(s_i)} \rangle_i$ obeys Gaussian distribution and the corresponding one-dimensional probability density function (PDF) can be written as

$$f_i^{(s_i)}(x) = \frac{1}{\sqrt{\pi N}} \exp\left(-\frac{\left(x - \left\langle i_o^{(s_i)} \right\rangle_i \right)^2}{N} \right). \tag{21}$$

And the one-dimensional PDF of interfering signal $\langle y_o^{(s_i)} \rangle_j$ can be represented as

$$f_j^{(s_i)}(x) = \frac{1}{\sqrt{\pi N}} \exp\left(-\frac{\left(x - \left\langle i_o^{(s_i)} \right\rangle_j \right)^2}{N} \right), \tag{22}$$

The probability that the envelopes of $f_j^{(s_i)}(x)$ do not exceed certain threshold h can be expressed with the help of [51] as

$$\begin{aligned} F_j^{(s_i)}(h) &= \int_{-\infty}^{h} f_j^{(s_i)}(x)\, \mathrm{d}x \\ &= 1 - 0.5\, \mathrm{erfc}\left[\left(h - \left\langle i_o^{(s_i)} \right\rangle_j \right) \Big/ \sqrt{N} \right]. \end{aligned} \tag{23}$$

On the basis of the soft-decision maximum likelihood estimation, if all envelopes of the $(M-1)$ interfering signals do not exceed h, no error decision will occur in the system. In other words, there will be decision error when one or more envelopes of the $(M-1)$ interfering signals exceed this threshold, and the probability of decision error can be calculated as follows:

$$G_e^{(s_i)}(h) = 1 - \prod_{j=1, j\neq i}^{M} F_j^{(s_i)}(h). \tag{24}$$

It is obvious that $G_e^{(s_i)}(h)$ is related to the value of h, which equals $\langle y_o^{(S_i)} \rangle_i$. At the sampling instant, for example, once $\langle y_o^{(S_i)} \rangle_j > \langle y_o^{(S_i)} \rangle_k$ ($k \neq j$ and $k \in [1, M]$), decision error will occur. Thus, the conditional probability of receiving s_i under transmitting s_i and receiving s_j under transmitting s_i can be written as

$$\begin{aligned} p(s_i|s_i) &= \int_{-\infty}^{+\infty} f_i^{(s_i)}(h)\left[1 - G_e^{(s_i)}(h)\right]\mathrm{d}h \\ &= \frac{1}{\sqrt{\pi}} \int_{-\infty}^{+\infty} \exp\left(h - \eta_{s_i,s_i} \langle G_n \rangle L \sqrt{\gamma_B}\right) \\ &\quad \times \prod_{k=1, k\neq i}^{M} \left[1 - 0.5\mathrm{erfc}\left(h - \eta_{s_k,s_i} \langle G_n \rangle L \sqrt{\gamma_B}\right)\right]\mathrm{d}h \end{aligned} \tag{25}$$

and

$$\begin{aligned} p(s_j|s_i) &= \int_{-\infty}^{+\infty} f_j^{(s_i)}(h) \prod_{k=1,\ k\neq j}^{M} F_k^{(s_i)}(h)\mathrm{d}h \\ &= \frac{1}{\sqrt{\pi}} \int_{-\infty}^{+\infty} \exp\left(h - \eta_{s_j,s_i} \langle G_n \rangle L \sqrt{\gamma_B}\right) \\ &\quad \times \prod_{k=1, k\neq j}^{M} \left[1 - 0.5\mathrm{erfc}\left(h - \eta_{s_k,s_i} \langle G_n \rangle L \sqrt{\gamma_B}\right)\right]\mathrm{d}h, \end{aligned} \tag{26}$$

respectively, where γ_B is the signal-noise-ratio (SNR) at the receiver and it is defined as the ratio between the average power of photocurrent and the total noise power under the non-turbulence condition. Thus, γ_B can be expressed as

$$\gamma_B(\mathrm{dB}) = 10\log_{10}\frac{P_T^2}{N}. \tag{27}$$

For an OAMSK-based communication system, under the ISI-free condition, the relationship between the information rate R_b and channel bandwidth B can be represented with the help of [52] as

$$\frac{R_b}{B} = \frac{\log_2(M)}{(1+\beta)}, \tag{28}$$

where β is the roll-off factor varying from 0 to 1. Then, SNR per bit can be expressed as

$$\gamma_b(\mathrm{dB}) = \gamma_B(\mathrm{dB}) - 10\log_{10}\left[\log_2(M)\right] + 10\log_{10}(1-\beta). \tag{29}$$

For the short-range oceanic weak turbulent communication system, the channel can be modeled as a discrete and memoryless channel. And a stochastic $M \times M$ channel matrix $\mathbf{P}$ with M input and output symbols can be denoted as

$$\mathbf{P} = \left\{p\left(s_j / s_i\right)\right\},\ i = 1, \ldots, M \text{ and } j = 1, \ldots M, \tag{30}$$

where $p(s_j/s_i) \geq 0$ and $\sum_{j=1}^{M} p(s_j/s_i) = 1$. The probability distribution vector of the input symbols is written as follows:

$$\mathbf{p_{s_i}} = (p_1, \ldots, p_M), p_i \geq 0 \text{ and } \sum_{k=1}^{M} p_k = 1. \tag{31}$$

Then, SER of the UWOC system can be expressed as

$$P_e = \sum_{i=1}^{M} \left[p_i \sum_{j=1, j\neq i}^{M} p\left(s_j / s_i\right) \right]. \tag{32}$$

Further, the channel capacity of this OAMSK modulation system can be evaluated on the basis of the obtained channel matrix **P**. With Shannon's theorem [53], the channel capacity could be expressed as

$$\begin{aligned} C(\mathbf{P}, \mathbf{p_{s_i}}) &= \max_{\{\mathbf{p_{s_i}}\}} \left[H(s_i) - H\left(s_j / s_i\right) \right] \\ &= \max_{\{\mathbf{p_{s_i}}\}} \left[\sum_{i=1}^{M} -p_i \log_2 p_i + \sum_{i=1}^{M} \sum_{j=1}^{M} p\left(s_j / s_i\right) p_i \log_2 p\left(s_j / s_i\right) p_i \right. \\ &\quad \left. - \sum_{i=1}^{M} \sum_{j=1}^{M} p\left(s_j / s_i\right) p_i \log_2 \sum_{k=1}^{M} p\left(s_j / s_k\right) p_k \right] \end{aligned} \tag{33}$$

where $H(s_i)$ and $H(s_j/s_i)$ represent the source entropy and conditional entropy, respectively. In this work, $C(\mathbf{P}, \mathbf{p_{s_i}})$ can be calculated by Blahut-Arimoto algorithm [54], [55].

3. Numerical Calculations and System Performance Analysis

In this section, the analytical results of the weak turbulence-induced variations in vortex LG beams are presented, and the performances of SER and channel capacity are also analyzed. The oceanic turbulence parameters are $\tau = -4$, $\varsigma = 10^{-3}$ m, and the propagation distance z is 30 m. The wavelength is 417 nm and the waist of LG beam is 0.002 m. The path loss L is assumed to be unity without loss of generality, and in practical applications it can be added to the total power in units of dB. It is assumed that the receiver aperture diameter is larger than $2\omega(z)\sqrt{|max(s_i)|}$ to maximize the received power and thus the power losses induced by the photodetector can be neglected. As is known, when the value of receiver aperture diameter is fixed, the largest radial function field of the LG beam, i.e., the maximum number of OAM modes, is limited [28]. Therefore, the maximum OAM mode of 20 is considered and the transmitted OAM modes fall in the range $S = [-20, 20]$ in this work.

Fig. 2 shows the fraction of energy of the original transmitted OAM modes m shifting into modes $n \in S$ under three weak turbulence conditions with C_n^2 equal to 10^{-15}, 10^{-14} and 10^{-13} $K^2m^{-2/3}$. In this work, the oceanic turbulence will become stronger with C_n^2 varying from 10^{-15} $K^2m^{-2/3}$ to 10^{-13} $K^2m^{-2/3}$ and in each turbulence condition, four examples with $m = \{0, 5, 10, 15\}$ are taken into account. As can be seen, greater value of C_n^2 will lead to the fact that the turbulence-induced energy diffusion from the original OAM mode into the adjacent modes is more severe, which confirms the correctness of our propagation model over weak turbulent ocean. Moreover, the energy diffusion is more obvious with the increase of m for different turbulence conditions. This is because that the larger the OAM mode is, the more unstable vortex beams' phase will be. Besides, it can be found that the energy diffusion will cause effective energy loses and some energy is shifted to the extrinsic interfering modes under different turbulence conditions. For instance, in Fig. 2(a), the histogram shows an energy loss of about 13.9% with $m = 15$ and a normalized shifted energy $\eta_{14,15}$ of about 0.07. While in Fig. 2(c), the energy loss of mode 15 is about 90% and the energy of the adjacent OAM modes (14 and 16) can achieve the same order of magnitude as the effective energy $\eta_{15,15}$.

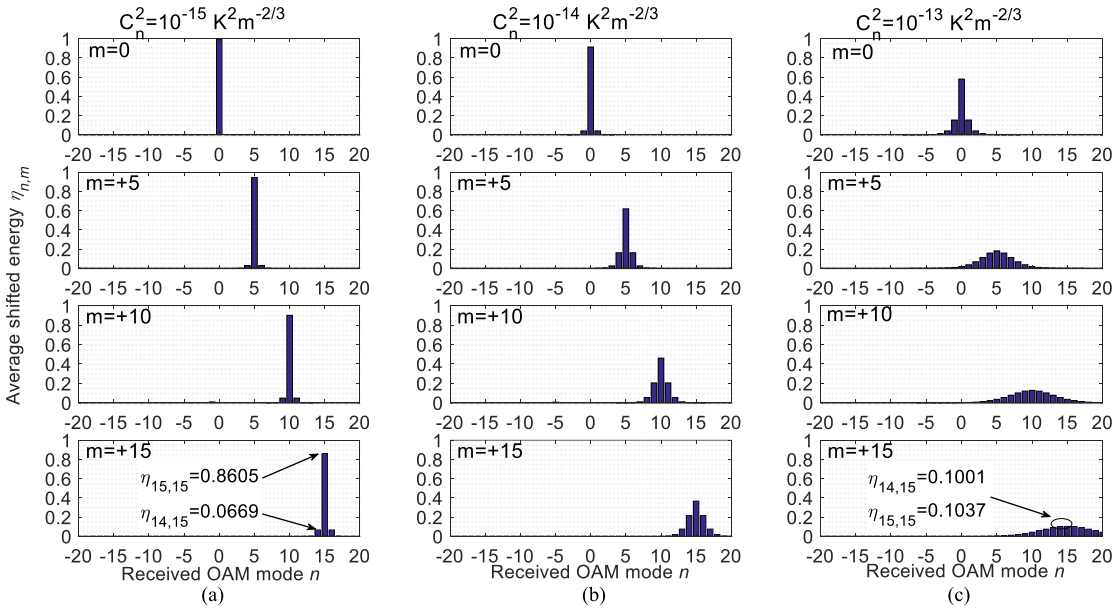

Fig. 2. Average projections of transmitted OAM modes $m = \{0, 5, 10, 15\}$ onto modes $n \in S$ after a propagation of 30 m in weak turbulent ocean: (a) $C_n^2 = 10^{-15}$ K^{2}m$^{-2/3}$, (b) $C_n^2 = 10^{-14}$ K^{2}m$^{-2/3}$, and (c) $C_n^2 = 10^{-13}$ K^{2}m$^{-2/3}$.

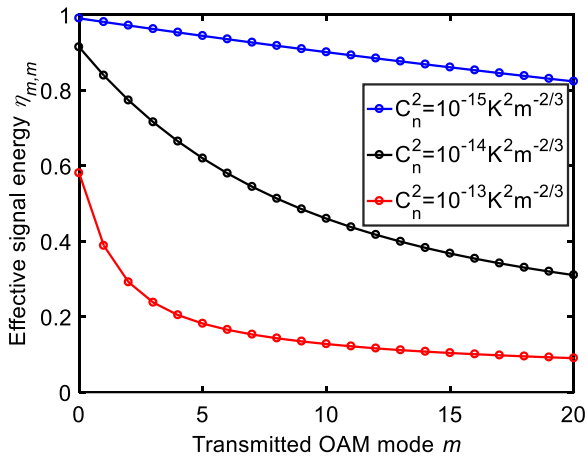

Fig. 3. Effective energy $\eta_{m,m}$ versus the transmitted OAM mode $m \in \{0, 1, \ldots, 19, 20\}$ for several values of weak oceanic turbulence condition.

Fig. 3 shows the variation of the effective energy $\eta_{m,m}$ with OAM mode m. As can be seen, as m increases, the values of $\eta_{m,m}$ will reduce under three weak turbulence conditions. For example, with $C_n^2 = 10^{-15}$ K^{2}m$^{-2/3}$, the curve can be fitted into a straight line with a slope of approximately -0.0083. With $C_n^2 = 10^{-13}$ K^{2}m$^{-2/3}$, $\eta_{m,m}$ decreases rapidly with the increasing m until it reaches 4. After that, $\eta_{m,m}$ decreases slowly and the curve can be fitted into a straight line with a smaller slope of about -0.0070. As is known from (19) and (26), the noise margin of this OAMSK modulation-based system is determined by the effective energy. That is, the decreasing effective energy due to the increasing m will degrade the reliability of UWOC system. Consequently, it would be best if the set S consists of small modes.

The average interfering energy of modes $m - \Delta m \in \{-4, -3, \ldots -1, 0, 1, \ldots, 15, 16\}$ shifted from the original transmitted OAM modes $m \in \{0, 1, \ldots, 19, 20\}$ are shown in Fig. 4 under three

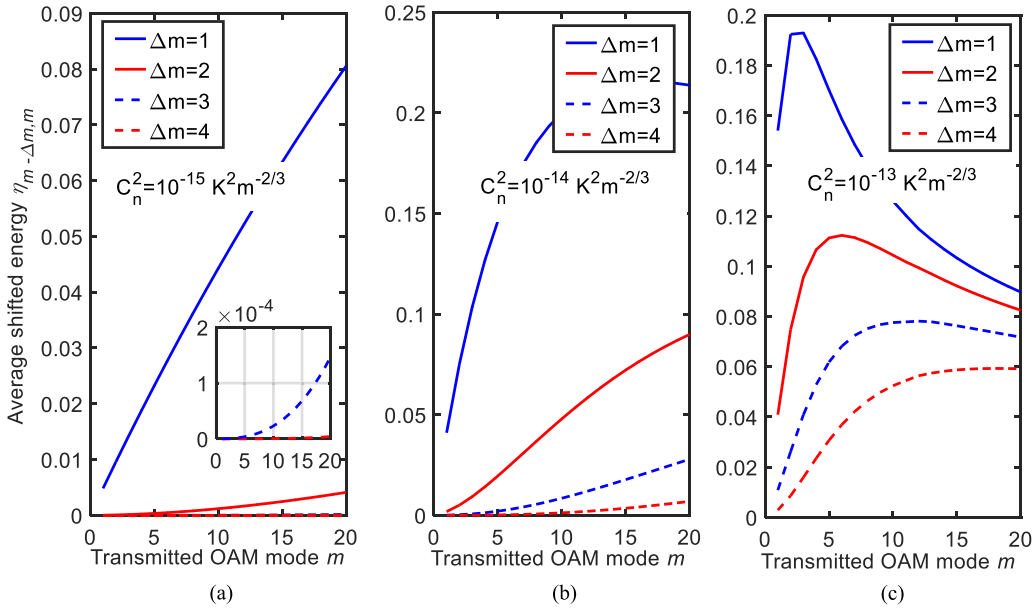

Fig. 4. Average interfering energy of $m - \Delta m \in \{-4, -3, \ldots - 1, 0, 1, \ldots, 15, 16\}$ versus the transmitted OAM mode $m \in \{0, 1, \ldots, 19, 20\}$ after propagating over weak turbulent ocean for turbulence conditions: (a) $C_n^2 = 10^{-15}$ K^{2}m$^{-2/3}$, (b) $C_n^2 = 10^{-14}$ K^{2}m$^{-2/3}$, and (c) $C_n^2 = 10^{-13}$ K^{2}m$^{-2/3}$.

oceanic turbulence conditions ($C_n^2 = 10^{-15}$, $C_n^2 = 10^{-14}$, and $C_n^2 = 10^{-13}$ K^{2}m$^{-2/3}$). As can be observed, the m-centered shifted energy with $\Delta m = 4$ is less than that with other mode intervals for all values of m in Fig. 3(a)–(c). This is because that the energy in one mode has a trend of spreading the energy onto its nearest modes [56]. As is known from (19), (26), and (32), decision error may occur when the energy of the extrinsic interfering signal increases. That is, the increase of the interfering energy due to the small Δm will degrade the SER performance of this UWOC system. Therefore, under the same turbulence condition, it would be the best if S with a larger interval is adopted to modulate the transmitted digital information. Here, it should be also noted that for all values of Δm, the average shifted energy increases with mode m for $C_n^2 = 10^{-15}$ K^{2}m$^{-2/3}$ in Fig. 3(a). However, a more complex variation tendency of the shifted energy for $C_n^2 = 10^{-13}$ K^{2}m$^{-2/3}$ scenario with the increasing m is shown in Fig. 3(c), especially for $\Delta m = 1, 2, 3$. It is obvious that these three curves rise at first and then go down with the increase of m. This is due to the fact that the unstable vortex beam's phase, which is caused by the increase of mode m and turbulence strength, will lead to more severe energy diffusion into the adjacent modes with larger interval. That is, with increasing m, more energy will shift to modes $m - 4$ and $m + 4$ and less energy will shift to modes $m - 1$ and $m + 1$.

For the M-ary OAMSK modulation-based UWOC system, S can be further expressed as $S = \{-\frac{M-1}{2}\Delta m + m_0, \ldots, -\Delta m + m_0, m_0, \Delta m + m_0, \ldots, \frac{M-1}{2}\Delta m + m_0\}$ for odd M and $S = \{-(\frac{M}{2} - 1)\Delta m + m_0, \ldots, -\Delta m + m_0, m_0, \Delta m + m_0, \ldots, \frac{M}{2}\Delta m + m_0\}$ for even M. As mentioned in Fig. 3, S should be comprised of small modes. Then, m_0 should be set to 0 and the minimum Δm should be adopted. However, as mentioned in Fig. 4, the large value of Δm should be considered to avoid the degradation of SER, while it is contrary to the conclusion of Fig. 3. Therefore, an optimum value of Δm cannot easily be determined and the selection of Δm requires a balance between the effects of decaying effective energy and the shifted interfering energy. In this work, to find the optimal Δm, the SERs with four values of Δm ($\Delta m = 1, 2, 3, 4$) are calculated. In particular, the optimal intervals are simulated in a limited range of [1], [4] because the largest mode is set to $|m| = 20$. Then, an optimal interval Δm can be achieved when the corresponding M-ary system reaches the SER of $P_e = 10^{-9}$ with the minimum amount of SNR per bit. The optimal intervals are summarized in Table 1 for three values of C_n^2 and seven values of M.

TABLE 1
Optimal intervals for M-ary OAMSK modulation UWOC system

C_n^2	OAM mode interval Δm						
	$M=2$	$M=3$	$M=4$	$M=5$	$M=6$	$M=7$	$M=8$
10^{-15} $K^2m^{-2/3}$	2	1	1	1	1	1	1
10^{-14} $K^2m^{-2/3}$	1	1	1	1	1	1	1
10^{-13} $K^2m^{-2/3}$	1, 2	1, 2	1	1	4	4	4

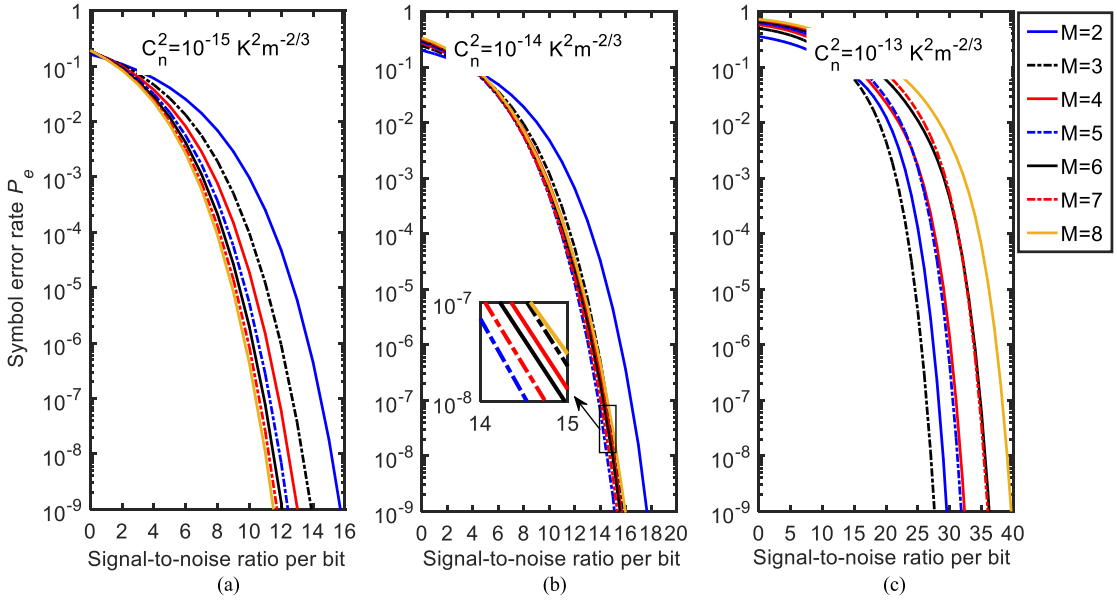

Fig. 5. SER P_e versus SNR per bit γ_b(dB) when optimal OAM mode interval is adopted in S for (a) $C_n^2 = 10^{-15}$ $K^2m^{-2/3}$, (b) $C_n^2 = 10^{-14}$ $K^2m^{-2/3}$, and (c) $C_n^2 = 10^{-13}$ $K^2m^{-2/3}$.

In Fig. 5, the SERs for OAMSK modulation-based UWOC system with the optimal Δm are plotted against the SNR per bit with different modulation orders M. As can be observed, the SER performance is sensitive to the variations in oceanic turbulence conditions. With $C_n^2 = 10^{-15}$ $K^2m^{-2/3}$, both the SERs and transmitted power consumption decrease with the increase of M. In this case, the value of M with the best SER performance is equal to 8. By making another tenfold increase in C_n^2, the SERs for all values of M except $M = 2$ are almost equal. As C_n^2 is further increased to 10^{-13} $K^2m^{-2/3}$ in Fig. 5(c), it can be seen that the SER performance is deteriorated and the required power consumption increases with the increase of M roughly. In this case, the value of M with the best SER performance equals 3. Besides, it can be found that the minimum amount of SNR per bit that is required to reach the SER of $P_e = 10^{-9}$ for the M-ary UWOC system increases much when the oceanic turbulence becomes stronger. For instance, for $C_n^2 = 10^{-15}$ $K^2m^{-2/3}$ the value of the minimum required SNR per bit is about 11 dB with $M = 8$, for $C_n^2 = 10^{-14}$ $K^2m^{-2/3}$ that is about 15 dB with $M = 5$, and for $C_n^2 = 10^{-13}$ $K^2m^{-2/3}$ that is about 26 dB with $M = 3$.

In Fig. 6, the channel capacities of OAMSK modulation-based UWOC system versus SNR γ_B are plotted. As can be seen, along with the increase of SNR, the channel capacity increases

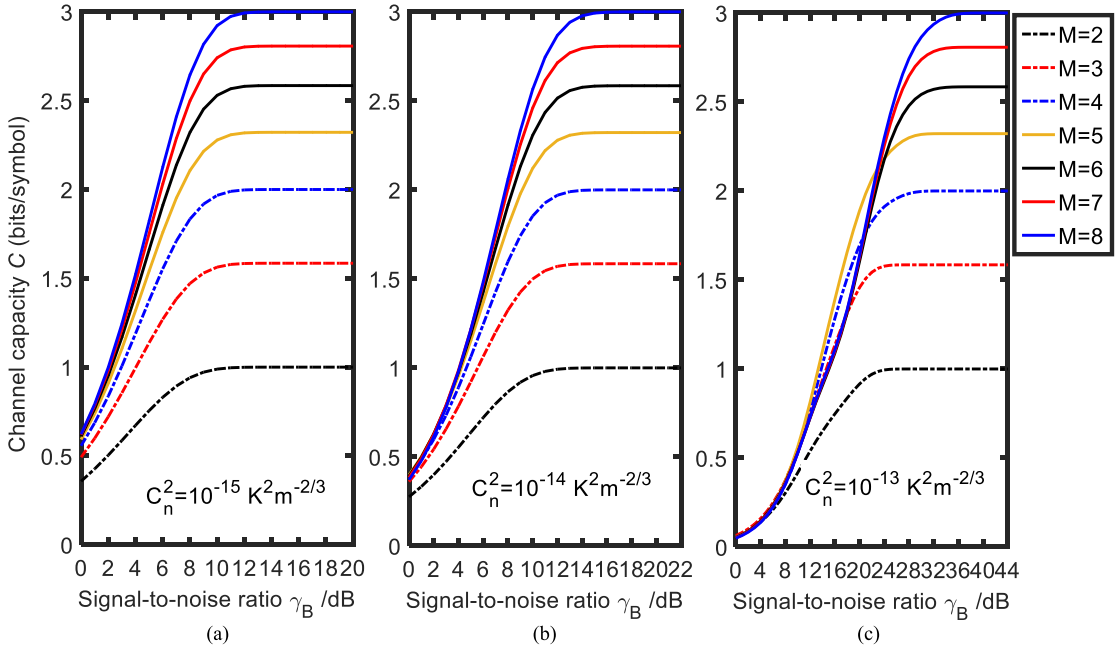

Fig. 6. Channel capacity C versus SNR $\gamma_B(dB)$ when optimal OAM mode interval is adopted in S with different M for (a) $C_n^2 = 10^{-15}$ K^{2}m$^{-2/3}$, (b) $C_n^2 = 10^{-14}$ K^{2}m$^{-2/3}$, and (c) $C_n^2 = 10^{-13}$ K^{2}m$^{-2/3}$.

approximately linearly at first and then reaches the saturation of $C_{max} = \log_2 M$ (bits/symbol), which confirms the correctness of our analytical channel capacity model. It can be also found that as M grows, the value of C will shift to a higher value at the same SNR after it reaches the saturation value under different turbulence conditions. Besides, for $C_n^2 = 10^{-15}$ K^{2}m$^{-2/3}$, it is known from Fig. 5(a) that increasing M will yield superior SER performance. Therefore, for a given value of SNR, a large modulation order can be adopted to improve the system capacity and SER performance. For $C_n^2 = 10^{-15}$ K^{2}m$^{-2/3}$, a similar conclusion can be achieved. However, for $C_n^2 = 10^{-13}$ K^{2}m$^{-2/3}$, it is known from Fig. 5(c) that increasing M may lead to a degradation of SER, which means that additional transmitted power is required for a fixed SER. Therefore, it is very important to balance the required transmitting power with the capacity gain to find an optimal M value for this case.

4. Conclusion

In summary, the performance of an M-ary UWOC system with OAMSK modulation was studied employing vortex LG beams propagating over weak turbulent ocean. The analytical expressions for SER and channel capacity of this system were derived, respectively. Under different weak turbulence conditions, the effects of energy diffusion-induced interfering energy and decaying effective energy on the selection of the optimal interval for the M-ary system were investigated in detail. With the optimal mode interval achieved, the SER performance and channel capacity for different modulation orders were then analyzed. The results showed that the variation in turbulence conditions remarkably affects the value of modulation order with the best SER performance, and to reach the SER of $P_e = 10^{-9}$, the minimum required transmitting power increases much when the oceanic turbulence becomes stronger. In addition, the capacity value will shift to a higher value with the increasing modulation order M, and a suitable M should be adopted to balance the transmitting power consumption and capacity gain. Furthermore, to enhance the performance of real UWOC system, OAMSK modulation scheme could be combined with MIMO and relay-assisted techniques because they are both easy-to-install and capable of significantly alleviate the underwater channel degrading effects.

References

[1] P. Tian, X. Liu, S. Yi, Y. Huang, S. Zhang, and X. Zhou, "High-speed underwater optical wireless communication using a blue GaN-based micro-LED," *Opt. Exp.*, vol. 25, no. 2, pp. 1193–1201, 2017.

[2] M. V. Jamali, A. Chizari, and J. Salehi, "Performance analysis of multi-hop underwater wireless optical communication systems," *IEEE Photon. Technol. Lett.*, vol. 29, no. 5, pp. 462–465, Mar. 2017.

[3] G. Qiao, Z. Babar, L. Ma, S. Liu, and J. Wu, "MIMO-OFDM underwater acoustic communication systems—A review," *Phys. Commun.*, vol. 23, pp. 56–64, 2017.

[4] L. Zhang, X. Xu, W. Feng, and Y. Chen, "Multi-array iterative receiver for underwater acoustic OFDM communications with EXIT chart evaluation," *Appl. Acoust.*, vol. 114, pp. 307–316, 2016.

[5] Y. Ren, L. Li, Z. Wang, S. M. Kamali, and E. Arbabi, "Orbital angular momentum-based space division multiplexing for high-capacity underwater optical communications," *Sci. Rep.*, vol. 6, 2016, Art. no. 33306.

[6] H. M. Oubei, R. Elafandy, K. Park, T. K. Ng, and M. S. Alouini, "Performance evaluation of underwater wireless optical communications links in the presence of different air bubble populations," *IEEE Photon. J.*, vol. 9, no. 2, 2017, Art. no. 7903009.

[7] M. V. Jamali, J. A. Salehi, and F. Akhoundi, "Performance studies of underwater wireless optical communication systems with spatial diversity: MIMO scheme," *IEEE Trans. Commun.*, vol. 65, no. 3, pp. 1176–1192, Mar. 2017.

[8] F. Akhoundi, M. V. Jamali, N. B. Hassan, H. Beyranvand, A. Minoofar, and J. A. Salehi, "Cellular underwater wireless optical CDMA network: Potentials and challenges," *IEEE Access*, vol. 4, pp. 4254–4268, 2016.

[9] M. V. Jamali, F. Akhoundi, and J. A. Salehi, "Performance characterization of relay-assisted wireless optical CDMA networks in turbulent underwater channel," *IEEE Trans. Wireless Commun.*, vol. 15, no. 6, pp. 4104–4116, Jun. 2016.

[10] Z. Zeng, S. Fu, H. Zhang, Y. Dong, and J. Cheng, "A survey of underwater optical wireless communications," *IEEE Commun. Surv. Tuts.*, vol. 19, no. 1, pp. 204–238, Jan./Mar. 2017.

[11] J. Baghdady *et al.*, "Multi-gigabit/s underwater optical communication link using orbital angular momentum multiplexing," *Opt. Exp.*, vol. 24, no. 9, pp. 9794–9805, 2016.

[12] H. M. Oubei, J. Duran, B. Janjua, and H. Y. Wang, "4.8 Gbit/s 16-QAM-OFDM transmission based on compact 450-nm laser for underwater wireless optical communication," *Opt. Exp.*, vol. 23, no. 18, pp. 23302–23309, 2015.

[13] P. Poirier and B. Neuner, "Undersea laser communication using polarization and wavelength modulation," *Appl. Opt.*, vol. 53, no. 11, pp. 2283–2289, 2014.

[14] S. Jaruwatanadilok, "Underwater wireless optical communication channel modeling and performance evaluation using vector radiative transfer theory," *IEEE J. Sel. Areas Commun.*, vol. 26, no. 9, pp. 1620–1627, Dec. 2008.

[15] W. C. Cox, B. L. Hughes, and J. F. Muth, "A polarization shift-keying system for underwater optical communications," in *Proc. Int. Conf. IEEE OCEANS*, Oct. 2009, pp. 1–4.

[16] M. Sui, X. Yu, and F. Zhang, "The evaluation of modulation techniques for underwater wireless optical communications," in *Proc. 2009 Int. Conf. IEEE Commun. Software Netw.*, 2009, pp. 138–142.

[17] I. B. Djordjevic, M. Arabaci, L. Xu, and T. Wang, "Spatial-domain-based multidimensional modulation for multi-Tb/s serial optical transmission," *Opt. Exp.*, vol. 19, no. 7, pp. 6845–6857, 2011.

[18] G. Gibson *et al.*, "Free-space information transfer using light beams carrying orbital angular momentum," *Opt. Exp.*, vol. 12, no. 22, pp. 5448–5456, 2004.

[19] L. Allen, M. W. Beijersbergen, R. J. C. Spreeuw, and J. P. Woerdman, "Orbital angular momentum of light and the transformation of Laguerre–Gaussian laser modes," *Phys. Rev.*, vol. 45, no. 11, pp. 8185–8189, 1992.

[20] A. Willner *et al.*, "Optical communications using orbital angular momentum beams," *Adv. Opt. Photon.*, vol. 7, no. 1, pp. 66–106, 2015.

[21] R. Y. Mesleh, H. Haas, S. Sinanović, C. WookAhn, and S. Yun, "Spatial modulation," *IEEE Trans. Veh. Technol.*, vol. 57, no. 4, pp. 2228–2241, Jul. 2008.

[22] G. Gibson *et al.*, "Free-space information transfer using light beams carrying orbital angular momentum," *Opt. Exp.*, vol. 12, no. 22, pp. 5448–5456, 2004.

[23] M. Krenn *et al.*, "Communication with spatially modulated light through turbulent air across Vienna," *New J. Phys.*, vol. 16, 2014, Art. no. 113028.

[24] J. Du and J. Wang, "High-dimensional structured light coding/decoding for free-space optical communications free of obstructions," *Opt. Lett.*, vol. 40, no. 21, pp. 4827–4830, 2015.

[25] A. J. Willner, Y. Ren, G. Xie, L. Li, and Y. Cao, "Free-space optical communications using encoding of data on different orbital-angular-momentum modes," *Proc. SPIE*, vol. 9739, 2016, Art. no. 97390.

[26] C. Kai, P. Huang, F. Shen, H. Zhou, and Z. Gou, "Orbital angular momentum shift keying based optical communication system," *IEEE Photon. J.*, vol. 9, no. 2, Apr. 2017, Art. no. 7902510.

[27] Y. Zhao and J. Wang, "High-base vector beam encoding/decoding for visible-light communications," *Opt. Lett.*, vol. 40, no. 21, pp. 4843–4846, 2015.

[28] J. A. Anguita, M. A. Neifeld, and B. V. Vasic, "Turbulence-induced channel crosstalk in an orbital angular momentum-multiplexed free-space optical link," *Appl. Opt.*, vol. 47, no. 13, pp. 2414–2429, 2008.

[29] M. Li, Z. Yu, and M. Cvijetic, "Influence of atmospheric turbulence on OAM-based FSO system with use of realistic link model," *Opt. Commun.*, vol. 364, no. 13, pp. 50–54, 2016.

[30] L. C. Andrews and R. L. Phillips, *Laser Beam Propagation Through Random Media*, 2nd ed. Bellingham, WA, USA: SPIE, 2005.

[31] L. Mandel and E. Wolf, *Optical Coherence and Quantum Optics*. Cambridge, U. K.: Cambridge Univ. Press, 1995.

[32] Y. Zhang *et al.*, "Influence of atmospheric turbulence on the transmission of orbital angular momentum for Whittaker-Gaussian laser beams," *Opt. Exp.*, vol. 22, no. 18, pp. 22101–22110, 2014.

[33] Y. Huang, B. Zhang, Z. Gao, G. Zhao, and Z. Duan, "Evolution behavior of Gaussian Schell-model vortex beams propagating through oceanic turbulence," *Opt. Exp.*, vol. 22, no. 15, pp. 17723–17734, 2014.

[34] V. V. Nikishov and V. I. Nikishov, "Spectrum of turbulent fluctuations of the sea-water refraction index," *Int. J. Fluid Mech. Res.*, vol. 27, no. 1, pp. 82–98, 2000.
[35] O. Korotkova and N. Farwell, "Effect of oceanic turbulence on polarization of stochastic beam," *Opt. Commun.*, vol. 384, no. 7, pp. 1740–1746, 2011.
[36] S. A. Thorpe, *The Turbulent Ocean*, Cambridge, U. K.: Cambridge Univ. Press, 2005.
[37] Y. Wu, Y. Zhang, Y. Li, and Z. Hu, "Beam wander of Gaussian-Schell model beams propagating through oceanic turbulence," *Opt. Commun.*, vol. 371, pp. 59–66, 2016.
[38] B. Cochenour, L. Mullen, and A. Laux, "Effects of multiple scattering on the implementation of an underwater wireless optical communication link, naval air systems command," in *Proc. Int. Conf. IEEE OCEANS*, Boston, MA, USA, Sep. 2006, pp. 1–6.
[39] S. Tang, Y. Dong, and X. Zhang, "Impulse response modeling for underwater wireless optical communication links," *IEEE Trans. Commun.*, vol. 62, no. 1, pp. 226–234, Jan. 2014.
[40] Y. Dong, J. Liu, and H. Zhang, "On capacity of 2-by-2 underwater wireless optical MIMO channels," in *Proc. Int. Conf. IEEE Adv. Wireless Opt. Commun.*, Riga, Latvia, Nov. 2015, pp. 219–222.
[41] W. C. Cox Jr., "Simulation, modeling, and design of underwater optical communication systems," Ph.D. dissertation, North Carolina State Univ., Raleigh, NC, USA, 2012. [Online]. Available: http://www.github.com/gallamine/ photonator
[42] S. R. Saunders, *Antennas and Propagation for Wireless Communication Systems*. New York, NY, USA: Wiley, 1999.
[43] M. V. Jamali, F. Akhoundi, and J. A. Salehi, "Performance characterization of relay-assisted wireless optical CDMA networks in turbulent underwater channel," *IEEE Trans. Wireless Commun.*, vol. 15, no. 6, pp. 4104–4116, Jun. 2016.
[44] W. Cox and M, John, "Simulating channel losses in an underwater optical communication system," *J. Opt. Soc. Amer. A*, vol. 31, no. 5, pp. 920–934, 2014.
[45] H. Zhang and Y. Dong, "Impulse response modeling for general underwater wireless optical MIMO links," *IEEE Commun. Mag.*, vol. 54, no. 2, pp. 56–61, Feb. 2016.
[46] L. Yang, W. Liu, and Z. Xu, "SIMO detection schemes for underwater optical wireless communication under turbulence," *Photon. Res.*, vol. 3, no. 3, pp. 48–53, 2015.
[47] J. W. Giles and I. N. Bankman, "Underwater optical communications systems. Part 2: Basic design considerations," in *Proc. Int. Conf. IEEE Mil. Commun.*, Atlantic, NJ, USA, Oct. 2005, pp. 1700–1705.
[48] M. V. Jamali and J. A. Salehi, "On the BER of multiple-input multiple-output underwater wireless optical communication systems," *IEEE Trans. Wireless Commun.*, vol. 15, no. 6, pp. 4104–4116, Jun. 2016.
[49] P. Wang, B. Yang, L. Guo, and T. Shang, "SER performance analysis of MPPM FSO system with three decision thresholds over exponentiated Weibull fading channels," *Opt. Commun.*, vol. 354, pp. 1–8, 2015.
[50] L. N. Binh, *Advanced Digital Optical Communication*, 2nd ed. Munich, Germany: CRC Press, 2015.
[51] C. Fan and L. Cao, *The Principle of Communication*. Beijing, China: Wiley, 2008.
[52] J. Boccuzzi, *Signal Processing for Wireless Communication*. New York, NY, USA: McGraw-Hill, 2007.
[53] C. Shannon, "A mathematical theory of communication," *Bell Syst. Tech. J.*, vol. 27, no. 3, pp. 379–423, 623–656, 1948.
[54] S. Arimoto, "An algorithm for computing the capacity of arbitrary discrete memoryless channels," *IEEE Trans. Inf. Theory*, vol. 18, no. 1, pp. 14–20, Jan. 1972.
[55] R. E. Blahut, "Computation of channel capacity and rate-distortion functions," *IEEE Trans. Inf. Theory*, vol. 18, no. 4, pp. 460–473, Jul. 1972.
[56] J. Zhou, J. Zong, and D. Liu, "Coupled mode theory for orbital angular momentum modes transmission in the presence of atmosphere turbulence," *Opt. Exp.*, vol. 23, no. 25, pp. 31964–31976, 2013.